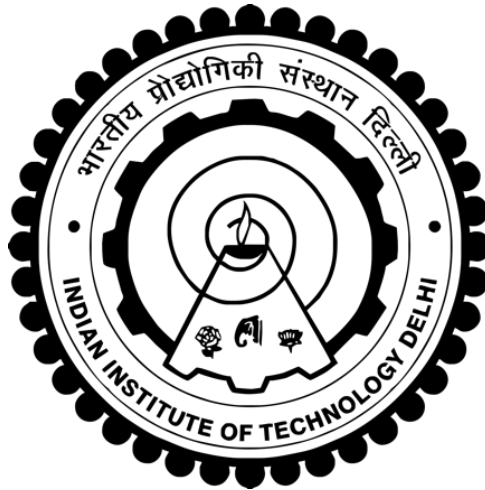


**LONG-TERM TREND OF CLOUD
FRACTION OVER THE INDIAN OCEAN IN
THE WARMING ERA**

JASWANT



**Centre for Atmospheric Sciences
Indian Institute of Technology Delhi**

June 2025

**© Indian Institute of Technology Delhi (IITD),
New Delhi, 2025**

Long-Term Trend of Cloud Fraction over the Indian Ocean in the Warming Era

by

Jaswant

Centre for Atmospheric Sciences

Submitted

**In fulfilment of the requirements of the degree of Doctor of
Philosophy**

To the



Indian Institute of Technology Delhi

June 2025

Certificate

This is to certify that the thesis entitled “Long-Term Trend of Cloud Fraction over the Indian Ocean in the Warming Era” being submitted by Jaswant for the award of the degree of Doctor of Philosophy, is a record of the original bonafide research work carried out by him. He has worked under my guidance and supervision and has fulfilled the requirements for submitting this thesis. The results presented in this thesis have not been submitted in part or whole to any University or Institution for the award of any degree/diploma.

Dr. Sagnik Dey

Professor

**Centre for Atmospheric Sciences,
Indian Institute of Technology Delhi,
Hauz Khas, New Delhi-110016, India**

Dr. Vimlesh Pant

Professor

**Centre for Atmospheric Sciences,
Indian Institute of Technology Delhi,
Hauz Khas, New Delhi-110016, India**

Acknowledgements

I would like to acknowledge and give my warmest thanks to my supervisors Dr. Sagnik Dey and Dr. Vimlesh Pant who made this work possible. Their guidance and support carried me through all stages of my PhD. I sincerely thank my SRC (Student Research Committee) members for generously sharing their knowledge and time. I would also like to thank the Head of the Centre, my CRC (Centre Research Committee) chairperson, and all the faculties and staff at the Centre for Atmospheric Sciences (CAS), Indian Institute of Technology Delhi, for providing all the necessary facilities and a great environment to learn and grow. During my Ph.D. tenure, they were always available for discussion, suggestions, and other academic and non-academic help.

I want to acknowledge the High-performance computing (HPC) facilities at the Indian Institute of Technology Delhi for providing the required computing facilities for extensive satellite data handling during my PhD tenure. I also acknowledge the computing and storage facilities at the Centre for Atmospheric Sciences, Indian Institute of Technology Delhi needed for hassle-free computation and analysis during my PhD. I sincerely thank the institute fellowship provided by the institute. I also acknowledge the student research travel assistance provided by the Indian Institute of Technology Delhi, which helped in covering the expenses for attending the international conferences. I want to acknowledge the Island of Meetings, ER Castiglione del Lago, Perugia, Italy for providing the National Institute of Geophysics and Volcanology grant to attend the 8th International School on Convective Volcanic Cloud Detecting, Monitoring and Modelling at Nicolosi, Italy.

I want to thank my friends, hostel mates, and lab mates from IIT Delhi for always being friends in need, and their excellent company made my stay at the institute pleasant and memorable. I also thank the SPICMACAY (The Society for the Promotion of Indian Classical Music And Culture Amongst Youth) club, and Nigiri Hostel for being part of my life during the PhD period.

Words cannot express my love and gratitude to my family, who supported and encouraged me through this journey. Their love and affection have been pillars of strength and a critical aspect of my life journey. My parents were my first teachers. They scolded and moulded me and gave me the freedom to become what I am today.

The final acknowledgement is dedicated to the almighty God and the Universe for bestowing me with passion, strength, perseverance, resources, curiosity and patience to pursue and complete the highest academic degree.

06/06/2025

Jaswant

Abbreviations

BOB	Bay of Bengal
CALIPSO	Cloud-Aerosol Lidar and Infrared Pathfinder Satellite Observations
CAPE	Convectively Available Potential Energy
CAS	Centre for Atmospheric Sciences
CCN	Cloud Condensation Nuclei
CF	Cloud Fraction
CLARA-A3	Third edition of the CM SAF cLoud, Albedo and surface RAdiation dataset from AVHRR
CMIP5	Coupled Model Intercomparison Project
CRC	Centre Research Committee
DJF	December-January-February
DMI	Dipole Mode Index
E	Evaporation
ECCRA	Extended Edited Synoptic Cloud Reports Archive
ECMWF	European Centre for Medium-Range Weather Forecasts
EIS	Estimated Inversion Strength

ENSO	El Niño-Southern Oscillation
ERA5	European Centre for Medium-Range Weather Forecasts fifth generation reanalysis
ESRL	Earth System Research Laboratory
g	Acceleration due to gravity
GOCCP	GCM-Oriented CALIPSO Cloud Product
GPCP	Global Precipitation Climatology Project
HadISST2	Hadley Centre Sea Ice and Sea Surface Temperature data set
HCF	High-Level Cloud Fraction
hPa	Hecto-Pascal
HPC	High-Performance Computing
IIT	Indian Institute of Technology
IOD	Indian Ocean Dipole
ISCCP	International Satellite Cloud Climatology Project
ISO	intra-seasonal oscillations
ITCZ	Inter-Tropical Convergence Zone
JJA	June-July-August

JRA55	Japanese 55-year Reanalysis
K	Kelvin
LCF	Low-Level Cloud Fraction
LST	Local Standard Time
LWCRF	Long-wave cloud radiative forcing
MAM	March-April-May
mb	Millibars
MCF	Mid-Level Cloud Fraction
MCST	Moderate Resolution Imaging Spectroradiometer Characterization Support Team
MFC	Moisture Flux Convergence
MERRA-2	Modern-Era Retrospective Analysis for Research and Applications, Version 2
MISR	Multi-angle Imaging SpectroRadiometer
MJO	Madden-Julian Oscillation
MODIS	Moderate Resolution Imaging Spectroradiometer
MSLP	Mean-Sea Level Pressure

MVIMD	Mean Vertically Integrated Moisture Divergence
NOAA	National Oceanic and Atmospheric Administration
OSTIA	Operational Sea Surface Temperature and Sea Ice Analysis
P	Precipitation
Pa	Pascals
q	Specific humidity
SON	September-October-November
SPICMAYCAY	Society for the Promotion of Indian Classical Music and Culture Amongst Youth
SRC	Student Research Committee
SST	Sea Surface Temperature
SWCRF	Short-wave cloud radiative forcing
TCmax	Time of Maximum Cloud Fraction
TOA	Top of the Atmosphere
TRMM	Tropical rainfall measuring mission
u	Zonal wind velocity

UTC	Coordinated Universal Time
v	Meridional wind velocity
V	Wind Velocity
VIEMF	Vertical Integral of Eastward Moisture Flux
VINMF	Vertical Integral of Northward Moisture Flux
w700	Vertical Wind at 700 hPa
Γ_m^{850}	Moist adiabatic lapse rate at 850 hPa
ρ	Density
$^{\circ}\text{C}$	Degrees Celsius
Z_{LCL}	Local altitude of 700 hPa
θ_{700}	Potential Temperature at 700 hPa
θ_{surf}	Potential Temperature at surface

Abstract

The long-term changes in clouds can lead to regional and global climate change. At present, the interaction of clouds with different earth system components is difficult to parametrise in the climate models. Hence, they are the major source of uncertainty in future climate projections. The key is to understand the long-term changes in cloud properties using observational datasets at a regional scale. Previous global and regional studies of clouds reported long-term trends in clouds up to 2009. However, the inadequacy of recent results and regional contrasts in results emphasise on the need to analyse the long-term trends in cloud properties at a regional scale and extend the analysis to the most recent years. Clouds over the Indian Ocean are vital for regional and global climate. Most cloud-related studies over the Indian Ocean are either of short study periods or focused on the cloud-aerosol-microphysical interaction, highlighting a need for studying long-term changes in clouds over the region. Among the micro- and macro-physical properties of clouds, cloud fraction (CF) stands out as a key parameter deriving the cloud-climate interaction. This study highlights the long-term changes and associated modulation of radiative feedback of CFs over the Indian Ocean.

Currently, all long-term CF datasets have limitations, ground-based and ship observation datasets suffer from limited temporal and spatial resolution and are not free from human bias. The satellite datasets often contain technical artefacts or are available for a short time duration, rendering them unsuitable for climate studies. European Centre for Medium-Range Weather Forecasts (ECMWF) fifth-generation reanalysis (ERA5) provides global three-dimensional CF data at $0.25^{\circ} \times 0.25^{\circ}$ spatial and hourly temporal resolution at 37 pressure levels for more than four decades, making it fit for climate studies. This study first evaluated the ERA5 CF against resolution-corrected Multi-angle Imaging Spectroradiometer (MISR), view-angle corrected Moderate Resolution Imaging Spectroradiometer (MODIS) and GCM-Oriented Cloud-Aerosol Lidar and Infrared Pathfinder Satellite Observations (CALIPSO) Cloud Product (CALIPSO-GOCCP) datasets.

The diurnal, seasonal, inter-annual and long-term variation of CF is evident over the Indian Ocean. During the period of the last four decades (1979-2018), the low-level CF (LCF) has decreased by 0.04, the mid-level CF (MCF) has increased by 0.05, and the high-level CF (HCF) has increased by 0.05-0.12 over the Indian Ocean. The observed changes in the CF has caused

a change in the LCF radiative feedback by $1.17 \times 10^{-3} \text{ Wm}^{-2}\text{K}^{-1}$ and a change in the MCF and HCF radiative feedback by $2.95 \times 10^{-3} \text{ Wm}^{-2}\text{K}^{-1}$ and $3.3 \times 10^{-3} \text{ Wm}^{-2}\text{K}^{-1}$ respectively. The temporal and spatial characteristics of all three types of clouds are well explained by sea surface temperature (SST). Additionally, a seasonally varying SST threshold between 28.5°C and 29°C for HCF is observed over the Indian Ocean, which has increased by 0.5°C in the last four decades. This study suggests that the overall warming and positive radiative feedback over the Indian Ocean is contributed by the long-term changes in the CF.

A novel ‘Diurnal Clock’ method has been used to scrutinise the seasonal and spatial patterns of the diurnal variations of CF in this study. The climatologically high values of LCF, MCF and HCF are observed to peak after midnight to morning hours, while the secondary values are observed to peak during afternoon to evening hours. The long-term changes in CF have altered the diurnal amplitude of clouds over the Indian Ocean. The diurnal amplitude of LCF has decreased, while the diurnal amplitudes of MCF and HCF have increased over the last four decades. The time of maximum CF (TCmax) over the Indian Ocean has also changed over the last four decades. The CF over the Indian Ocean shows an increase during midnight to morning hours and a decrease during the afternoon to evening hours. These results have important implications for the local energy budget and hydrological cycle.

All three types of clouds exhibited inter-annual variability from September to November (SON) period, with the highest inter-annual variability shown by HCF. This study asserts that inter-annual variability of CF over the Indian Ocean is predominantly governed by the direct and indirect consequences of mean-sea level pressure (MSLP) anomalies of the subtropical high. The CF increases over the western side during the positive phase of the Indian Ocean dipole (IOD) and El Niño. Conversely, the CF increases over the eastern side during the negative phase of IOD and La Niña. The inter-annual anomalies of CF over the eastern side of the Indian Ocean are governed by a mixed effect of SST and moisture convergence anomalies, while governed by moisture convergence anomalies over the western part of the Indian Ocean. During the positive phase of IOD and ENSO, the coastal upwelling and shallowing of thermocline near the Indonesian Coast is triggered by the basin-scale spatial spread of MSLP

anomalies. During the negative phase of IOD and ENSO, moisture over the eastern part of the basin is transported by the strong westerly wind anomalies near the equator.

In summary, the long-term changes of low-, mid-, and high-level CFs and the associated modulation of radiative feedback are highlighted in this study. The long-term changes in the diurnal amplitude of clouds are associated with long-term changes in the CF over the Indian Ocean. There has been a shift in the tendency of clouds to peak after midnight to morning hours as compared to afternoon to evening hours, and this transition suggests plausible changes in the diurnal temperature range, regional warming and changes in the precipitation patterns. Apart from the diurnal and long-term changes, clouds over the Indian Ocean are also affected by the IOD, ENSO and dynamics of subtropical high causing inter-annual variations in the spatial patterns of CF. The results of this study suggest the role of contrasting trends of CF in positive radiative feedback over the Indian Ocean.

Future research should expand the analysis by including a broader set of cloud-controlling variables to better understand the mechanism behind cloud formation and variability. Comparative modelling studies could be conducted to validate the cloud radiative feedback results obtained in this study. Additionally, the diurnal clock method could be applied to investigate the diurnal variation of clouds over other regions of the Indian Ocean, providing a more comprehensive view. Future work might also focus on identifying the underlying causes for the observed shift in the TCmax, particularly over the Bay of Bengal (BOB) region.

सारांश

बादलों में दीर्घकालिक परिवर्तन क्षेत्रीय और वैश्विक जलवायु परिवर्तन का कारण बन सकते हैं। वर्तमान में, जलवायु मॉडलों में विभिन्न पृथ्वी प्रणाली घटकों के साथ बादलों की परस्पर क्रिया को सांकेतिक रूप से दर्शाना कठिन है। अतः वे भविष्य की जलवायु अनुमानों में प्रमुख अनिश्चितता का स्रोत हैं। मुख्य बात यह है कि क्षेत्रीय स्तर पर अवलोकनात्मक आंकड़ों का उपयोग करके बादलों के गुणों में दीर्घकालिक परिवर्तन को समझना। पिछले वैश्विक और क्षेत्रीय अध्ययनों में 2009 तक बादलों में दीर्घकालिक रुझानों की जानकारी दी गई है। हालांकि, हालिया परिणामों की अपर्याप्तता और क्षेत्रीय विरोधाभासों के कारण क्षेत्रीय स्तर पर बादलों की विशेषताओं में दीर्घकालिक रुझानों का विश्लेषण करने और इसे हाल के वर्षों तक विस्तारित करने की आवश्यकता पर बल दिया गया है। हिन्द महासागर के ऊपर बादल क्षेत्रीय और वैश्विक जलवायु के लिए अत्यंत महत्वपूर्ण हैं। हिन्द महासागर पर अधिकांश बादल संबंधी अध्ययन या तो छोटे अध्ययन अवधि के होते हैं या बादल-एयरोसोल-सूक्ष्म भौतिकीय अंतःक्रिया पर केंद्रित होते हैं, जिससे इस क्षेत्र में बादलों के दीर्घकालिक परिवर्तनों के अध्ययन की आवश्यकता स्पष्ट होती है। बादलों के सूक्ष्म- और स्थूल-भौतिक गुणों में, बादल अंश (CF) एक प्रमुख पैरामीटर के रूप में उभरता है जो बादल-जलवायु अंतःक्रिया को निर्धारित करता है। यह अध्ययन भारतीय महासागर पर CF के दीर्घकालिक परिवर्तनों और उनसे संबंधित विकिरणीय प्रतिपुष्टि के संशोधन को उजागर करता है।

वर्तमान में, सभी दीर्घकालिक CF डेटासेट्स में सीमाएँ हैं। भूमि आधारित और जहाज से प्राप्त अवलोकन डेटासेट्स सीमित समयिक और स्थानिक विभेदन से ग्रस्त होते हैं और मानव पूर्वाग्रह से मुक्त नहीं होते। उपग्रह डेटासेट्स में अक्सर तकनीकी त्रुटियाँ होती हैं या वे केवल सीमित समय अवधि के लिए उपलब्ध होते हैं, जिससे वे जलवायु अध्ययन के लिए अनुपयुक्त हो जाते हैं। यूरोपीय मध्यकालीन मौसम पूर्वानुमान केंद्र (ECMWF) की पांचवीं पीढ़ी का पुनःविश्लेषण (ERA5) 37 दबाव स्तरों पर $0.25^{\circ} \times 0.25^{\circ}$ स्थानिक और प्रति घंटा समयिक सटीकता के साथ वैश्विक तीन-आयामी CF डेटा प्रदान करता है, जो चार दशकों से अधिक का डेटा उपलब्ध कराता है, इसलिए यह जलवायु

अध्ययन के लिए उपयुक्त है। इस अध्ययन में सबसे पहले ERA5 CF का, रिज़ॉल्यूशन-सुधारित मल्टी-एंगल इमेजिंग स्पेक्ट्रोरेडियोमीटर (MISR), व्यू-एंगल-सुधारित मॉडरेट रिज़ॉल्यूशन इमेजिंग स्पेक्ट्रोरेडियोमीटर (MODIS) और GCM-उन्मुख क्लाउड-एयरोसोल लिडार और इन्फ्रारेड पाथफाइंडर सैटेलाइट ऑब्जर्वेशन्स (CALIPSO) क्लाउड प्रोडक्ट (CALIPSO-GOCCP) डेटा सेट्स के साथ मूल्यांकन किया गया है।

हिंद महासागर पर CF का दैनिक, मौसमी, अंतर-वर्षीय और दीर्घकालिक परिवर्तन स्पष्ट रूप से देखा जा सकता है। पिछले चार दशकों (1979-2018) के दौरान, निम्न-स्तरीय बादल अंश (LCF) में 0.04 की कमी आई है, मध्य-स्तरीय बादल अंश (MCF) में 0.05 की वृद्धि हुई है, और उच्च-स्तरीय बादल अंश (HCF) में 0.05-0.12 की वृद्धि हुई है। CF में देखे गए परिवर्तनों के कारण LCF विकिरणीय प्रतिपुष्टि में $1.17 \times 10^{-3} \text{ Wm}^{-2}\text{K}^{-1}$ का परिवर्तन और MCF और HCF विकिरणीय प्रतिपुष्टि में क्रमशः $2.95 \times 10^{-3} \text{ Wm}^{-2}\text{K}^{-1}$ और $3.3 \times 10^{-3} \text{ Wm}^{-2}\text{K}^{-1}$ का परिवर्तन हुआ है। सभी तीन प्रकार के बादलों की समयिक और स्थानिक विशेषताएँ समुद्र की सतह तापमान (SST) द्वारा अच्छी तरह से स्पष्ट होती हैं। इसके अतिरिक्त, हिंद महासागर HCF के लिए 28.5°C और 29°C के बीच एक मौसमी रूप से परिवर्तित SST सीमा देखी जाती है, जो पिछले चार दशकों में 0.5°C बढ़ी है। यह अध्ययन सुझाव देता है कि हिंद महासागर पर समग्र गर्मी और सकारात्मक विकिरणीय प्रतिक्रिया, CF में दीर्घकालिक परिवर्तनों के कारण होती है।

इस अध्ययन में CF की दैनिक विविधताओं के मौसमी और स्थानिक पैटर्न की जांच करने के लिए एक नवीन विचार 'डायरनल क्लॉक' का उपयोग किया गया है। LCF, MCF और HCF के जलवायु संबंधी उच्च मान आधी रात से सुबह के घंटों के दौरान चरम पर देखे गए हैं, जबकि द्वितीयक मान दोपहर से शाम के घंटों के दौरान चरम पर देखे गए हैं। CF में दीर्घकालिक परिवर्तनों ने हिंद महासागर के ऊपर बादलों के दैनिक आयाम को बदल दिया है। पिछले चार दशकों में LCF के दैनिक आयाम में कमी आई है, जबकि MCF और HCF के

दैनिक आयाम में वृद्धि हुई है। पिछले चार दशकों में हिंद महासागर पर अधिकतम CF का समय (TCmax) भी बदल गया है। हिंद महासागर के ऊपर CF मध्यरात्रि से सुबह के समय में वृद्धि और दोपहर से शाम के समय के दौरान कमी दर्शाता है। इन परिणामों का स्थानीय ऊर्जा बजट और जल विज्ञान चक्र पर महत्वपूर्ण प्रभाव पड़ता है।

सभी तीन प्रकार के बादलों ने सितंबर से नवंबर (SON) अवधि के दौरान अंतर-वार्षिक परिवर्तनशीलता प्रदर्शित की, जिसमें HCF द्वारा दर्शाई गई उच्चतम अंतर-वार्षिक परिवर्तनशीलता थी। यह अध्ययन दावा करता है कि हिंद महासागर पर CF की अंतर-वार्षिक परिवर्तनशीलता मुख्य रूप से उपोष्णकटिबंधीय उच्च के औसत-समुद्र स्तर दबाव (एमएसएलपी) विसंगतियों के प्रत्यक्ष और अप्रत्यक्ष परिणामों से नियंत्रित होती है। हिंद महासागर द्विध्रुव (IOD) और अल नीनो के सकारात्मक चरण के दौरान CF पश्चिमी तरफ बढ़ता है। इसके विपरीत, आईओडी और ला नीना के नकारात्मक चरण के दौरान CF पूर्वी हिस्से में बढ़ जाता है। हिंद महासागर के पूर्वी हिस्से में CF की अंतर-वार्षिक विसंगतियाँ SST और नमी अभिसरण विसंगतियों के मिश्रित प्रभाव से नियंत्रित होती हैं, जबकि हिंद महासागर के पश्चिमी भाग में नमी अभिसरण विसंगतियों द्वारा नियंत्रित होती हैं। IOD और ENSO के सकारात्मक चरण के दौरान, इंडोनेशियाई तट के पास थर्मोकलाइन का तटीय उत्थान और उथलापन MSLP विसंगतियों के बेसिन-स्केल स्थानिक प्रसार से शुरू होता है। IOD और ENSO के नकारात्मक चरण के दौरान बेसिन के पूर्वी भाग में भूमध्य रेखा के पास तेज़ पश्चिमी हवा की विसंगतियों द्वारा नमी का परिवहन होता है।

संक्षेप में, इस अध्ययन में निम्न-, मध्य- और उच्च-स्तरीय CF के दीर्घकालिक परिवर्तन और विकिरण प्रतिपुष्टि के संबंधित मॉड्यूलेशन पर प्रकाश डाला गया है। बादलों के दैनिक आयाम में दीर्घकालिक परिवर्तन हिंद महासागर के ऊपर CF में दीर्घकालिक परिवर्तनों से जुड़े हैं। दोपहर से शाम के घंटों की तुलना में आधी रात के बाद सुबह के घंटों में बादलों के चरम पर पहुंचने की प्रवृत्ति में बदलाव आया है, और इस बदलाव के कारण दैनिक तापमान सीमा में

बदलाव, क्षेत्रीय वार्मिंग और वर्षा के पैटर्न में बदलाव हो सकता है। दैनिक और दीर्घकालिक परिवर्तनों के अलावा, हिंद महासागर पर बादल IOD, ENSO और उपोष्णकटिबंधीय उच्च की गतिशीलता से भी प्रभावित होते हैं, जिससे CF के स्थानिक पैटर्न में अंतर-वार्षिक बदलाव होता है। इस अध्ययन के नतीजे हिंद महासागर पर सकारात्मक विकिरण प्रतिक्रिया में CF के विपरीत रुझानों की भूमिका का सुझाव देते हैं।

भविष्य के अनुसंधान में बादल निर्माण और परिवर्तनशीलता के पीछे के तंत्र को बेहतर ढंग से समझने के लिए बादल-नियंत्रक चर की एक व्यापक श्रृंखला को शामिल करके विश्लेषण का विस्तार करना चाहिए। इस अध्ययन में प्राप्त बादल विकिरण प्रतिक्रिया के परिणामों को मान्य करने के लिए तुलनात्मक मॉडलिंग अध्ययनों का संचालन किया जा सकता है। इसके अतिरिक्त, दैनिक घड़ी पद्धति का उपयोग हिंद महासागर के अन्य क्षेत्रों में बादलों की दैनिक परिवर्तनशीलता की जांच के लिए किया जा सकता है, जिससे एक अधिक व्यापक दृष्टिकोण प्राप्त किया जा सके। भविष्य के कार्य में विशेष रूप से बंगाल की खाड़ी (BOB) क्षेत्र में देखे गए TCmax के बदलाव के अंतर्निहित कारणों की पहचान पर भी ध्यान केंद्रित किया जा सकता है।

Contents

Certificate	4
Acknowledgements	5
Abbreviations	7
Abstract	12
सारांश	15
Contents	19
List of Figures	23
Chapter 1. Introduction	29
1.1 Importance of clouds in the climate system	30
1.2 CF as a key climate variable	30
1.3 Previous studies on long-term changes in CF	31
1.4 Cloud-related studies over the Indian Ocean	32
1.5 Research gap and motivation	34
1.6 Thesis objectives and thesis structure	34
Chapter 2. Data and methodology	36
2.1 Introduction of ERA5 dataset	37
2.2 Validation of the CF dataset	39
2.2.1 Resolution corrected MISR dataset	40
2.2.2 View-angle corrected MODIS dataset	40
2.2.3 GCM-Oriented CALIPSO Cloud Product (GOCCP)	41
2.2.4 Third edition of the CM SAF cCloud, Albedo and surface RAdiation dataset from AVHRR (CLARA-A3)	41
2.2.5 Modern-Era Retrospective Analysis for Research and Applications (MERRA-2)	41

2.2.6 Japanese 55-year Reanalysis (JRA55)	42
2.2.7 Comparison statistics of ERA5 CF with other cloud products	42
2.3 Meteorological variables	44
2.3.1 Estimated Inversion Strength	45
2.3.2 Vertical wind at 700 hPa	47
2.3.3 Sea surface temperature	48
2.3.4 Air temperature at 2 m from the surface	49
2.3.5 Convective available potential energy	49
2.3.6 Mean sea level pressure	50
2.3.7 Mean vertically integrated moisture divergence	50
2.3.8 Vertical integral of eastward moisture flux	52
2.3.9 Vertical integral of northward moisture flux	52
2.3.10 IOD and ENSO indices	52
2.4 Diurnal clock method	53
2.5 Moisture budget analysis	54
2.5 Radiative feedback framework	55
Chapter 3. Long-term trend and variability of clouds and their vertical distribution over the Indian Ocean	59
3.1 Seasonal variation of CF, SST and winds over the Indian Ocean	60
3.1.1 Seasonal climatology of CF over the Indian Ocean	60
3.1.2 Seasonal climatology of SST and wind speed over the Indian Ocean	62
3.2 Impact of SST on CF over the Indian Ocean	63
3.2.1 Impact of SST on low-level CF over the Indian Ocean	63
3.2.2 Impact of SST on mid-level CF over the Indian Ocean	67
3.2.3 Impact of SST on high-level CF over the Indian Ocean	69
3.3 Impact of EIS on low-level CF over the Indian Ocean	76
3.4 Impact of w700 on mid-level CF over the Indian Ocean	79
3.5 Impact of CAPE on high-level CF over the Indian Ocean	83
3.6 Long-term trend in the vertical profile of the CF over the Indian Ocean	87
3.7 Changes in the local cloud feedback over the Indian Ocean	94

3.8 Summary	94
Chapter 4. Diurnal variation of CF over the northern Indian Ocean	96
4.1 Diurnal variation of CF over the northern Indian Ocean	97
4.2 Diurnal variation of LCF over the Arabian Sea and BOB	97
4.2.1 Diurnal variation of LCF over the Arabian Sea	97
4.2.2 Diurnal variation of LCF over the BOB	98
4.3 Diurnal variation of MCF over the northern part of the Indian Ocean	102
4.3.1 Diurnal variation of MCF over the Arabian Sea	102
4.3.2 Diurnal variation of MCF over the BOB	103
4.4 Diurnal variation of HCF over the Arabian Sea and BOB	105
4.5 Change in the diurnal amplitude of CF over the Arabian Sea and BOB	107
4.5.1 Change in the diurnal amplitude of CF over the Arabian Sea	107
4.5.2 Change in the diurnal amplitude of CF over the BOB	108
4.5.3 Summary of change in the diurnal amplitude of CF over the Arabian Sea and BOB	108
4.5 Modulation in time of maximum CF	112
4.5.1 Spatial climatology of the time of maximum CF over the Arabian Sea and BOB	112
4.5.2 Modulation of the time of maximum CF over the Arabian Sea and BOB	115
4.6 Summary	118
Chapter 5. Impact of IOD and ENSO on the variation of CF over the Indian Ocean during the post-monsoon season	119
5.1 Impact of IOD and ENSO on CF over the Indian Ocean	120
5.2 Inter-annual variability of CF over the Indian Ocean	120
5.2.1 Composite analysis of CF over the Indian Ocean	120
5.2.2 Correlation between HCF and SST anomalies over the Western and Eastern Box	121
5.2.3 Correlation between the HCF and CAPE anomalies over the Indian Ocean	125
5.3 Composites of moisture transport over the Indian Ocean	125
5.4 Composites of MSLP over the Indian Ocean	126

5.5 Connection with the seasonal migration of subtropical high	127
5.6 Summary	133
Chapter 6. Thesis summary and future direction	134
6.1 Summary	135
6.2 Limitations of the study	143
6.3 Future scope of the study	144
References	145
Publications	150
Brief Bio-data	151

List of Figures

Figure 2.1 Statistical comparison between the dummy CF data with a spurious trend (a) and ERA5 total CF (b) over the Indian Ocean. The top left plot shows the area-averaged trend (blue) and regression line (red), and the top right plot shows residuals of the trend (green). The bottom left plot shows the histogram of residuals with a normal fit line (red) and the bottom right plot shows the 5-year rolling average slope of residuals (red).....	38
Figure 2.2 Spatial comparison (a), linear correlation (b), and box plot comparison (c) statistics between the total CF from ERA5 and resolution corrected MISR dataset (2000-2017) at 10:30 local standard time (LST).	43
Figure 2.3 Spatial climatology of total CF from ERA5 (left column) and MODIS (right column) at 10:30 LST (2002-2017).	46
Figure 2.4 Seasonal correlation statistics between total CF at 10:30 AM from ERA5 and MODIS datasets (2002-2017).	47
Figure 2.5 Comparison between vertical CF of ERA5 data and CALIPSO-GOCCP (2007-2018). The Longitudinally averaged profile of CF (a) and the latitudinally averaged profile of CF (b) are shown by the left and right panels.	48
Figure 2.6 Linear fitting of CF time-series with scatter plot and histogram of the residuals about the trend line using ERA5 data over the Indian Ocean (1979-2018).....	51
Figure 2.7 Correlation of cloud radiative forcing with HCF (a & b), MCF (c & d) and LCF (e & f) over the Indian Ocean using ERA5 dataset (1979-2018).....	57
Figure 3.1 Seasonal climatology of ERA5 CF (unitless) for low-level (left column), mid-level (middle column), and high-level (right column) clouds for the period 1979-2018 in DJF, MAM, JJA, and SON, respectively (from top to bottom).	61

Figure 3.2 Seasonal climatology of (a) 10 m wind speed (ms^{-1}) and (b) Sea Surface Temperature ($^{\circ}\text{C}$) over the Indian Ocean using ERA5 dataset (1979-2018). The colour contours represent respective magnitudes, and arrows indicate wind speed vectors (magnitude and direction). .64

Figure 3.3 Temporal linear correlation between the low-level CF and sea surface temperature over the Indian Ocean using ERA5 dataset (1979-2018). The statistically significant locations above 95% are stippled using black dot marks.66

Figure 3.4 Schematics of the temporal evolution of low-level CF (top right) along the diagonal from the coast of Somalia to the northern part of the Arabian Sea (top left). Schematic of temperature inversion with height along the diagonal for MAM (bottom left) and for JJA (bottom right).67

Figure 3.5 Temporal linear correlation between the mid-level CF and sea surface temperature over the Indian Ocean using the ERA5 dataset (1979-2018). The statistically significant locations above 95% are stippled using black dot marks.68

Figure 3.6 Temporal linear correlation between the high-level CF and sea surface temperature over the Indian Ocean using the ERA5 dataset (1979-2018). The statistically significant locations above 95% are stippled using black dot marks.71

Figure 3.7 Correlation between the SST and CF bins for MCF (a) and HCF (b) over the Indian Ocean using ERA5 dataset from 1979-2018. The NaN represents the absence of data or non-significant correlation below 95%. The first row (0-1) of cloud fraction bins in the vertical axis shows the correlation between the SST and CF of entire range between 0 to 1, the second row (0.1-1) represents the same over the regions of CF values strictly above 0.1, and so on.72

Figure 3.8 Spatial distribution of HCF bins number count (vertical axis) and underlying SST (horizontal axis) over the Indian Ocean for the initial (dotted lines) and final decade (solid lines) of the study period (1979-2018).73

Figure 3.9 Spatial distribution of high-level (a) and mid-level clouds (b) with underlying SST over the Indian Ocean using cloud product from ISCCP-h series dataset and SST from ERA5 dataset.74

Figure 3.10 Temporal distribution of MCF bins (a) and HCF bins (b) over the Indian Ocean. Temporal distribution and cross-correlation sequence (c) between the highest value MCF and HCF bin over the Indian Ocean using ERA data (2018). 75

Figure 3.11 Seasonal climatology of Estimated Inversion Strength (EIS) over the Indian Ocean using ERA5 dataset (1979-2018). 77

Figure 3.12 Temporal linear correlation between EIS and SST over the Indian Ocean using ERA5 dataset (1979-2018). The statistically significant locations above 95% are stippled using black dot marks. 78

Figure 3.13 Spatial correlation between the EIS with different LCF ranges over the Indian Ocean using the ERA5 dataset (1979-2018). The first row (0-1) of cloud fraction bins in the vertical axis shows the correlation between the EIS and CF of entire range between 0 to 1, the second row (0.1-1) represents the same over the regions of CF values strictly above 0.1, and so on..... 79

Figure 3.14 Climatology of vertical wind at 700 hPa over the Indian Ocean using ERA5 dataset (1979-2018). The negative values denote upward motion, while positive values show downward motion. 80

Figure 3.15 Correlation between vertical wind at 700 hPa and MCF over the Indian Ocean using ERA5 dataset (1979-2018). The statistically significant locations above 95% are stippled using black dot marks. 81

Figure 3.16 Spatial correlation between the w700 and different LCF ranges over the Indian Ocean using ERA5 dataset (1979-2018). The first row (0-1) of cloud fraction bins in the vertical axis shows the correlation between the w700 and CF of entire range between 0 to 1, the second row (0.1-1) represents the same over the regions of CF values strictly above 0.1, and so on. 82

Figure 3.17 Spatial climatology of CAPE over the Indian Ocean using ERA5 data (1979-2018). 84

Figure 3.18 Temporal linear correlation between CAPE and high-level CF over the Indian Ocean using ERA5 data (1979-2018). The statistically significant locations above 95% are stippled using black dot marks..... 85

Figure 3.19 Spatial correlation between the CAPE and different HCF ranges over the Indian Ocean using ERA5 dataset (1979-2018). The first row (0-1) of cloud fraction bins in the vertical axis shows the correlation between the CAPE and CF of entire range between 0 to 1, the second row (0.1-1) represents the same over the regions of CF values strictly above 0.1, and so on. 86

Figure 3.20 Vertical profiles of seasonal trends (in year⁻¹) of fc over the Indian Ocean using ERA5 reanalysis dataset. Statistically significant (at 95% CI) trends are marked by dots.89

Figure 3.21 The trend of low-, mid-, and high-level CF over the Indian Ocean using ERA5 data (1979-2018). The statistically significant locations above 95% are stippled using black dot marks.....90

Figure 3.22 (a) Time series of de-seasoned and normalised CF, (b) quantile statistics of changes in seasonal CF over the Indian Ocean in the last four decades using the monthly ERA5 reanalysis dataset (1979-2018).91

Figure 4.1 Seasonal variation in the diurnal cycle of LCF over the (a) Arabian Sea and (b) Bay of Bengal using ERA5 dataset (1979-2018). The concentric circles in the diurnal clock diagrams represent the diurnal variation of LCF bins. The number on the circumference of the outer circles represents the local time. The diurnal variation of the lowest CF bin is represented in the smallest circle and the highest CF bin with an outermost circle. The colour values in a particular CF bin represent the normalised frequency according to the colour bar.....99

Figure 4.2 Diurnal variation of the vertical profile of temperature gradient (°C/hPa) averaged along the diagonal stretching from the Somalian Coast (50°E/10°N) to the northern border of the Arabian Sea (65°E/23°N), similar to Figure 3.4. The two merged colour schemes were used to enhance the presence of peak inversion time..... 100

Figure 4.3 The vertical profile of meridional wind (a & b), vertical velocity (c & d) and air temperature gradient (e & f) over the diagonal from 5N/79E to 23N/94E as shown in the cartoon (bottom right corner)..... 101

Figure 4.4 Seasonal variation in the diurnal cycle of MCF over the (a) Arabian Sea and (b) Bay of Bengal using ERA5 dataset (1979-2018). The schematics of the figure remains same as Figure 4.1. 104

Figure 4.5 Seasonal variation in the diurnal cycle of HCF over the (a) Arabian Sea and (b) Bay of Bengal using ERA5 dataset (1979-2018). The schematics of the figure remains same as Figure 4.1. 106

Figure 4.6 Seasonal climatology of the normalised diurnal amplitude of low-, mid-, and high-level clouds over the (a) Arabian Sea and (b) Bay of Bengal using ERA5 reanalysis data (1979-2018). 109

Figure 4.7 Change in the diurnal amplitude (Present – Past) of low, mid, and high-level clouds over the Arabian Sea in different seasons. The above 95% statistically significant areas are stippled with a black dot mark. The present decade is 2009-2018, and the past period is 1979-1988). 110

Figure 4.8 Change in the diurnal amplitude (Present – Past) of low, mid, and high-level clouds over the Bay of Bengal in different seasons. The above 95% statistically significant areas are stippled with a black dot mark. The present decade is 2009-2018, and the past period is 1979-1988). 111

Figure 4.9 Seasonal climatology of time of maximum CF (LST) for low-, mid-, and high-level clouds over the Arabian Sea using ERA5 data (1979-2018). 113

Figure 4.10 Seasonal climatology of time of maximum CF (LST) for low-, mid-, and high-level clouds over the Bay of Bengal using ERA5 data (1979-2018). 114

Figure 4.11 Change in the time of maximum CF for the low-level, mid-level, and high-level clouds over the Arabian Sea. The vertical axis in the bar plot shows the change in the number of data points. The legend represents the seasons. 116

Figure 4.12 Change in the time of maximum CF for the low-level, mid-level, and high-level clouds over the Bay of Bengal. The vertical axis in the bar plot shows the change in the number of data points. The legend represents the seasons. 117

Figure 5.1 Spatial (a) and area-averaged (b) values of inter-annual variability of annual low-, mid-, and high-level clouds over the Indian Ocean using ERA5 reanalysis dataset for the SON season (1979-2018). 122

Figure 5.2 Composites of low-, mid-, and high-level CF difference between the positive and negative phases of IOD (left column) and ENSO (right column) using ERA5 dataset during the SON season (1979-2018). 123

Figure 5.3 Scatter plot of correlation between monthly anomalies of SST and high-level CF over the east box (90°E-110°E and 10°S-0°N) and west box (50°E-70°E and 10°S-10°N) during the positive and negative phases of IOD (a) and ENSO (b). 124

Figure 5.4 Spatial correlation between the convective available potential energy and high-level CF anomalies during IOD (top row) and ENSO (bottom row). The statistically significant locations above 95% are stippled using black dot marks. 129

Figure 5.5 Composites of moisture flux convergence due to climatological mean state (upper row) and stationary eddies (anomaly, bottom row) for IOD (a) and ENSO (b) over the Indian Ocean. The positive values indicate divergence, and the negative values show convergence of moisture..... 130

Figure 5.6 Composites of moisture flux due to mean state (upper row) and stationary eddies (anomaly, bottom row) during the IOD (a) and ENSO (b) over the Indian Ocean 131

Figure 5.7 Composites of mean sea-level pressure (a) and mean sea-level pressure anomaly (b) during IOD and ENSO over the Indian Ocean. The overlaid arrows represent the climatology (a) and anomaly of wind speed and direction during the positive and negative phases of IOD and ENSO. 132